Journal of Alloys and Compounds 743 (2018) 87–98

Contents lists available at ScienceDirect

Journal of Alloys and Compounds

journal homepage: http://www.elsevier.com/locate/jalcom

Abnormal deformation behavior and particle distribution during hot compression of fine-grained 14 vol% SiCp/2014Al composite

Z.Y. Huang [a, b], X.X. Zhang [a], C. Yang [a, b], B.L. Xiao [a, *], Z.Y. Ma [a]

[a] Shenyang National Laboratory for Materials Science, Institute of Metal Research, Chinese Academy of Sciences, 72 Wenhua Road, Shenyang, 110016, China
[b] School of Materials Science and Engineering, University of Science and Technology of China, 72 Wenhua Road, Shenyang, 110016, China

ARTICLE INFO

Article history:
Received 9 November 2017
Received in revised form
26 January 2018
Accepted 30 January 2018
Available online 1 February 2018

Keywords:
Metal matrix composites
Plastic deformation
High-temperature properties
Particle distribution
Electron backscatter diffraction (EBSD)

ABSTRACT

The compressive deformation behavior of an extruded 14 vol% SiCp/2014Al composite fabricated by stir casting was investigated at temperatures of 355–495 °C and strain rates of 0.001–1 s^{-1}. An abnormal variation of flow stress with temperature was observed at low strain rates. This anomalous behavior was attributed to abnormal grain growth in the matrix alloy above a critical temperature, resulting in higher deformation resistance of the composite at elevated temperatures. Furthermore, the effect of the compression parameters on the particle distribution was investigated by the marked trace lines. It was indicated that after hot deformation, the particle free bands (PFBs) were commonly observed in the hard-to-deform region and shear deformation region. Increasing temperature and strain rate hardly improved particle distribution uniformity, while large compressive strain could eliminate the PFBs.

1. Introduction

In the past half century, the processing, mechanical properties and microstructures of silicon-carbide (SiC) particulate reinforced Al matrix composites (PRAMCs) have been extensively studied [1–6]. Although the PRAMCs generally exhibit low ductility, it is possible for the PRAMCs to undergo secondary processing if the reinforcement volume fraction is less than 40% [7]. The presence of SiC particles makes the composite be more prone to internal damage (such as debonding, cracking or particle fracture) than unreinforced metals, thus the secondary processing is generally conducted at elevated temperatures where the matrix alloy does not exhibit work-hardening behavior.

During the hot deformation of the PRAMCs the distribution of reinforcing particles varies with the plastic flow of matrix alloy. At the same time, the reinforcing particles also significantly affect the microstructural evolution of matrix alloy. An accurate understanding of deformation behavior is helpful to select appropriate processing parameters for fabricating the composite components with particular microstructures, thereby enhancing service performances (e.g., superior creep resistance and high-temperature strength).

Hot deformation is a dynamic process, and generally the stress-strain curves can be regarded as a manifestation of the deformation mechanisms of the PRAMCs. So far, the corresponding relationship between the shape of flow stress curves and the microstructural evolution for the PRAMCs has been rarely investigated in detail.

Generally, the strength of metallic materials decreases with increasing temperature. However, there exists exception in a few of alloys. For instance, in some Al-Li alloys [8,9] and their single crystalline alloys [10], at temperatures from −200 to 150 °C dislocations move in pairs cutting the δ'-Ll_2 precipitates, and the resistance to the motion of the super-dislocations by the δ'-particles enhances with increasing temperature, which leads to a positive temperature dependence of yield stress. In some nickel-based alloys [11,12], Kear-Wilsdorf locks, formed during screw dislocation cross-slip from {111} plane to {010} plane, multiply with increasing temperature. As a consequence, the yield strength increases with temperature.

The anomalous stress-temperature relationships have also been found in the PRAMCs [13], but the relevant mechanisms have not been explained concurrently. Compared to unreinforced aluminum alloys, the particles have significant effect on the microstructures of the matrix during hot working, thereby resulting in more complicated microstructural evolution. Therefore, the effect of microstructural evolution on the deformation behavior of the PRAMCs

* Corresponding author.
E-mail address: blxiao@imr.ac.cn (B.L. Xiao).

https://doi.org/10.1016/j.jallcom.2018.01.397
0925-8388/

should be carefully investigated.

Compared with the unreinforced alloys, an important microstructural evolution of the PRAMCs is the re-distribution of particles during hot deformation, which has a strong effect on the mechanical properties of the composite. The cluster or inhomogeneous distribution of reinforcing particles can promote the nucleation and propagation of cracks [14–16]. In contrast, the uniform distribution of particles can enhance ultimate tensile strength and elongation [3,17], and improves fatigue performance [18,19]. However, during hot working (e.g., forging or rolling) the effect of processing parameters on the uniformity of particle distribution has received few attentions.

In the present work, extrusion bars of stir cast 14 vol% SiCp/2014Al composite was subjected to hot compression tests. The reversed relationship between flow stress and temperature was observed and explained on the basis of microstructure evolution. Zener equation was taken into account to evaluate the stability of grain size during hot deformation. Furthermore, the effect of processing parameters and local stress and strain states on the distribution of particles was investigated in detail.

2. Experimental

The composite used in this study was 14 vol% SiC particle reinforced 2014Al (SiCp/2014Al) composite with a nominal particle size of 20 μm. The nominal chemical composition of 2014Al is Al-4.8Cu-0.6Mg-0.7Mn-0.7Fe-0.9Si [20]. The composite was fabricated by stir cast technique and subsequent extrusion which were described in references [21]. Details of the processing technique are considered to be proprietary by the manufacturer. The extruded bars were machined into cylindrical specimens 8 mm in diameter and 12 mm in height with the axis parallel to the extrusion direction.

The isothermal compression tests were conducted in temperature range from 355 °C to 495 °C with a temperature interval of 35 °C and at strain rates of 0.001, 0.01, 0.1 and 1.0 s^{-1} using the Gleeble-3800. Tantalum sheets 100 μm thickness were used to prevent adhesion between the end surfaces of cylindrical specimens and the anvils. The specimens were compressed to an ultimate true strain of 0.9. After hot compression, the specimens were water quenched immediately to retain the deformed microstructure. The specimens were cut through the centerline along the compression direction for microstructure examinations.

The samples for optical microscope (OM) were mechanically polished and etched using Keller's reagent, then observed by stereo microscopy (SM; Zeiss Stemi 2000-C), optical microscopy (OM; Zeiss Axiovert200 MAT). Electron back-scattered diffraction analysis was used to characterize grain boundaries orientation and confirm the OM examination. The specimens for electron back-scatter diffraction (EBSD) were firstly mechanically polished, and were ion milled using a beam milling system (IBMS; Lecia EM RES101). The EBSD analysis was conducted using a field emission scanning electron microscopy (FESEM; Zeiss Supra 55).

3. Results and discussion

3.1. Initial microstructure

Fig. 1 shows the microstructure of the as-received composite. The distribution of SiC particles was characterized by string-like arrays with the orientation of most aligned SiC particles parallel to the extrusion direction (Fig. 1a) and the substantial recrystallized microstructure was observed in the matrix with most of the

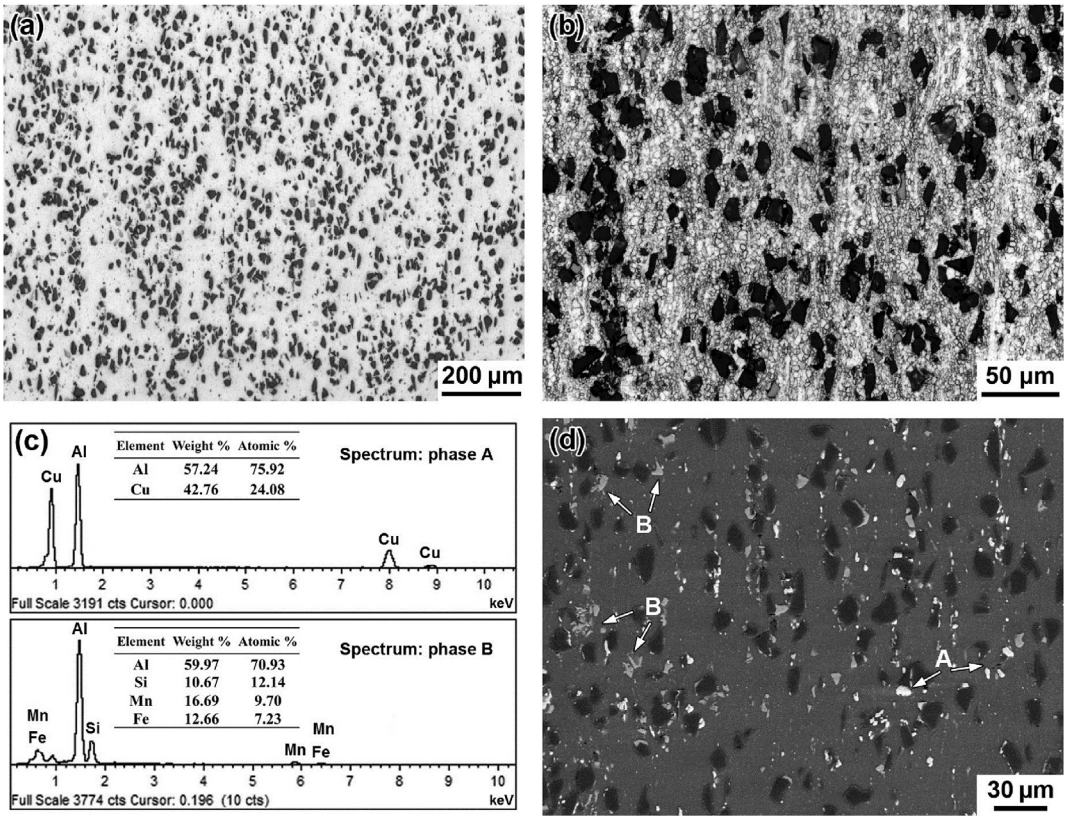

Fig. 1. Initial microstructure of the as-received 14 vol% SiCp/2014Al extrusion bars: (a) distribution state of SiC particles, (b) fine-grained configuration of matrix alloy, (c) SEM/EDS of precipitated phases, (d) SEM backs-scattered electron image (Extruded direction is perpendicular to the horizontal.).

recrystallized grains being equiaxed, except for some narrow and long grains (Fig. 1b). The average grain size of the matrix was determined to be about 2.5 μm, which is close to the lower limited subgrain size (~2 μm) of aluminum alloys at elevated temperatures [22].

The SEM/EDS (Fig. 1c) analyses disclosed that there were two main microstructural constituents in the composite. As shown in Fig. 1d, phase A could be determined to be $CuAl_2$ with smooth profile and white color, while phase B could be determined to be α-Al(Fe, Mn)Si with polyhedral shape and grey color, according to previous report [23].

3.2. Deformation behavior of fine-grained composite

3.2.1. Flow behavior

Fig. 2 shows the true stress versus true strain curves of the 14 vol % SiCp/2014Al composite during hot compression. In Fig. 2a, the flow stress increases with increasing strain rate at 425 °C. The same tendency existed at the other test temperatures. At the initial deformation stage, the flow stress curves in strain rates of 0.01–1 s^{-1} exhibit a peak followed by a stress decrease, which is related to the restoration processes of dislocations, substructures or grain boundaries referred to as dynamic recovery (DRV) or dynamic recrystallization (DRX). However, the curve at 0.001 s^{-1} and 425 °C exhibits a continuous increase in the stress after the yield point. The temperature of 425 °C and strain rate of 0.001 s^{-1} are close to the creep conditions [24,25]. The creep hardening rate is higher at the incipient deformation stage and then decreased. As a result, the flow stress increases slowly with continuous deformation.

In Fig. 2b, the flow stress curves at different temperatures exhibit a small strain interval between the upper and lower yield points at strain rate of 0.01 s^{-1}. After the yield point, the curves at 355 °C and 390 °C have a steady softening and a flat trend up to strain of 0.6, and then both curves subsequently turn into work hardening. However, at 425 °C, 460 °C and 495 °C all the flow curves exhibit a strain hardening after the yield point. In addition, the flow stress at 460 °C is close to that at 425 °C for a strain rate of 0.01 s^{-1}. This result might be related to the microstructure transformation as the temperature increases.

3.2.2. Anomalous increase of stress at higher temperature and low strain rate

The flow stress increases anomalously at temperatures higher than 425 °C for a low strain rate of 0.001 s^{-1}, as shown in Fig. 3. At the initial stage of deformation, the yield strength at 460 °C and 495 °C is higher than that at 425 °C. When strain reaches 0.4, the flow stress at 460 °C decreases to be below that at 425 °C.

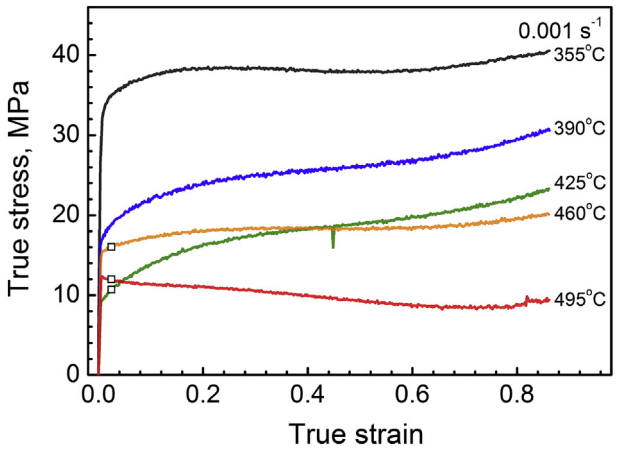

Fig. 3. True stress vs. true strain curves of 14 vol% SiCp/2014Al composites at strain rate 0.001 s^{-1} for different temperatures.

In order to understand the reverse stress-temperature relationship, the microstructures of the specimens at relevant deformation parameters with strains of 0.025 and 0.9 were examined. In Fig. 4a, the specimen compressed at 425 °C to a true strain of 0.025 had an average grain size of ~3.4 μm which is larger than that of the as-received composite (Fig. 1b). When deformed to a true strain of 0.9, as shown in Fig. 4b, the grain size increased slightly and was measured to be about 3.6 μm. These results were attributed to the dynamic grain growth (DGG) which was classified as dynamic recrystallization (DRX).

Fig. 4c shows that abnormal grain growth (AGG) occurred in the matrix at 460 °C with a small strain of 0.025. The coarsened grains were observed in most areas on the cross-section of the specimen except for the regions with SiC particle clusters. Fine-grained structure remained in the cluster zones since relative high contents of SiC particles constrained grain boundary migration during AGG. As the strain increased to 0.9, the large grains after AGG were refined significantly due to the following DRX process. Fig. 4d shows that a large number of low angle grain boundaries (LAGBs, shown as white lines) existed in the grain interiors. Fig. 4e shows that coarsened grains appeared even in the SiC cluster zones of deformed specimen at 495 °C with strain of 0.025, attributed to the further increase of grain boundary mobility at 495 °C. In this case, when strain increased to 0.9 (Fig. 4f) the grains were refined relatively homogeneously with a higher proportion of high angle grain

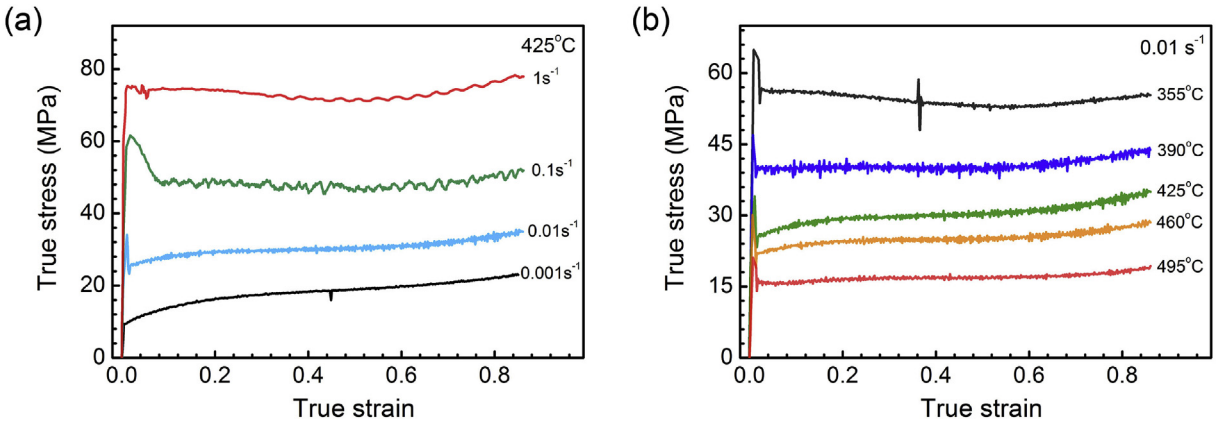

Fig. 2. True stress vs. true strain curves of 14 vol% SiCp/2014Al composites: (a) at 425 °C and variant strain rates, (b) at strain rate of 0.01 s^{-1} and variant temperatures.

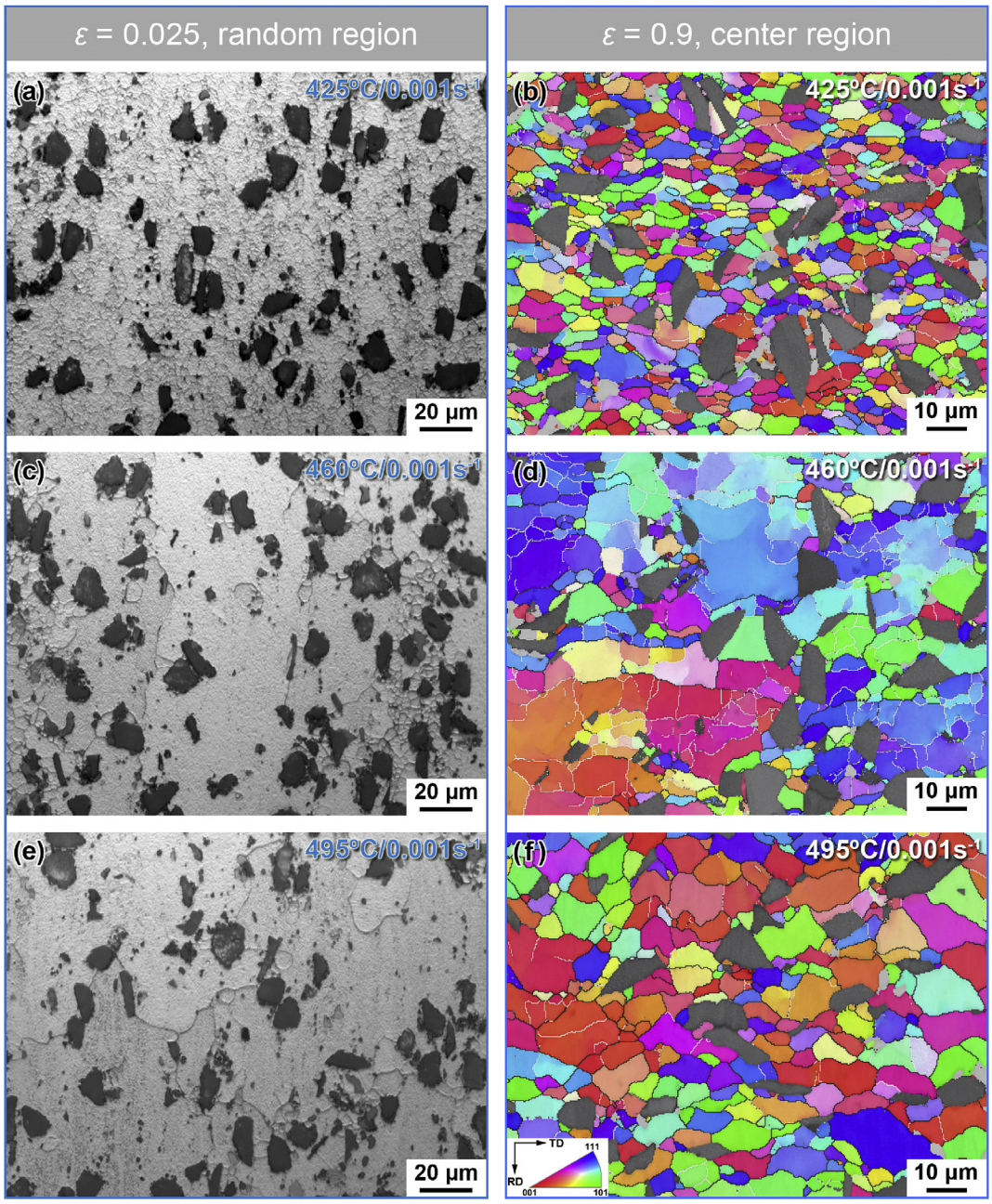

Fig. 4. Microstructure of the specimens compressed under strain rate 0.001 s^{-1}: (a) random region at 425 °C, (b) central region at 425 °C, (c) random region at 460 °C, (d) central region at 460 °C, (e) random region at 495 °C, (f) central region at 495 °C. Compressive direction is perpendicular to the horizontal. (b), (d), (f) are EBSD maps (IPF color + grain boundary, high angle grain boundaries (>15°) are marked by black lines and low angle boundaries (2–15°) are marked by white lines; SiC particles are shown by dark gray; $CuAl_2$ is shown by light gray.). (For interpretation of the references to color in this figure legend, the reader is referred to the Web version of this article.)

boundary (HAGB). Meanwhile, the spacing between particles and clusters reduced compared to the situation at lower strain of 0.025, implying that SiC particles was homogenously distributed at higher strain.

The above results suggest that there existed a critical temperature of AGG (T_{agg}) between 425 °C and 460 °C during hot working in the present fine grain composite. The T_{agg} was identified to be around 440 °C in our previous work [26]. As the temperature exceeded this critical point, grains grew immediately at the initial stage of plastic deformation. In addition, comparing the center region (Fig. 4d and f) with the shear region (Fig. 5a and b) of the compressed specimens, it is clearly noted that the grain sizes were remarkably different in the case of AGG. At the initial deformation stage AGG occurred throughout the whole specimen. As strain increased, the coarsened grains were refined at high strain since DRX occurred in the central region which was subjected to the maximum strain. In the shear deformation region, the coarsened grains still remained even at high applied strain due to relatively low local strain in this region. As shown in Fig. 5c and d, the number of LAGBs increased near the center region where the strain was larger.

The deformation conditions at 0.001 s^{-1} in Fig. 3 are close to the creep condition [24,25]. During creep deformation, strength of grain boundaries decreases apparently with increasing temperatures [27]. Moreover, Kottada et al. [28] suggested that the deformation under low stress occurred in the absence of significant

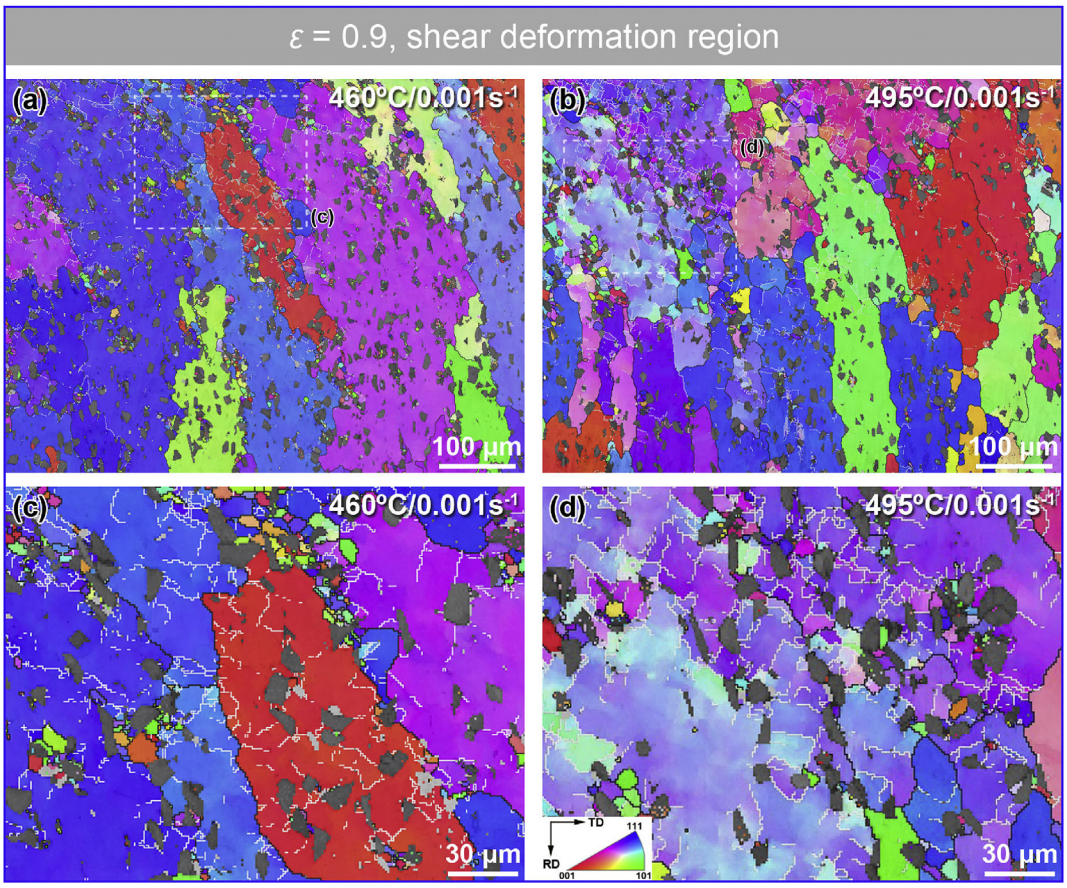

Fig. 5. EBSD maps (IPF color + grain boundary) in shear deformation region of the specimens compressed with true strain 0.9: (a) at 460 °C/0.001 s^{-1}, (b) at 495 °C/0.001 s^{-1}, (c) local region in the dotted box of (a), (d) local region in the dotted box of (b) (Compressive direction is perpendicular to the horizontal.). (For interpretation of the references to color in this figure legend, the reader is referred to the Web version of this article.)

Table 1
Average diameter and volume fraction of SiC reinforcement and second-phase particles.

Particulates	Average diameter (μm)	Volume fractions (%)
SiCp	17.1	14
$CuAl_2$	4.28	0.84
α-Al(Fe, Mn)Si	5.80	1.75
All particles	16.24 (volume-weighted)	16.59 (total)

intragranular dislocation movement, which was classified as diffusion creep. Under this creep regime, grain boundary sliding (GBS) made a large contribution to plastic deformation. In contrast, the high stresses generally corresponded to dislocation creep which is associated with more active intragranular dislocation behavior. Thus, the grain size has a significant influence on creep resistance. Obviously, the occurrence of AGG above 440 °C hindered GBS. In this case, the intragranular slip would contribute significantly to the overall strain. However, the intragranular slip was impeded by the SiC particles distributed in grain interior. It can be seen from Fig. 5c and d that a number of LAGBs were distributed around SiC particles and HAGBs, which was a consequence of the obstacle of intragranular SiC particles and the inhomogeneous stresses transmitted from neighboring grains during intragranular slip.

It is well known that reinforcement can impede grain growth of matrix alloys. Recent studies [29,30] disclosed that the nano scale reinforcement could effectively inhibit grain growth even if the initial grain was very fine. Compared to the composite, grain growth often took place in the unreinforced alloys during deformation at elevated temperatures [31,32]. In this reported studies, the grain growth ratio was about 4–6 times of size of original grains, and GBS could operate during deformation and the dependence of stress on temperature was normal. In both of cases, the anomalous increase of stress with rising temperature did not occur. By contrast, in the present composite, the large grain growth ratio up to 20–50 times inhibited GBS. Meanwhile, as shown by Fig. 5c and d, intragranular slip was impeded by intragranular SiC particles. Both the impediments were responsible for the anomalous increase of stress with rising temperature at low strain rate and high temperature.

3.2.3. *Dependence of flow curve shapes on microstructures*

Generally, the center regions of specimens made main contributions to the overall plastic deformation, the microstructures of center regions therefore had a stronger relevance to the flow curves. Except for the anomalous variation of flow stress with temperature, Figs. 3 and 4 also disclose variant flow behaviors at the same strain rate of 0.001 s^{-1} and different temperatures due to the microstructure evolution, which can be explained as follows:

(1) The flow stress curve at 425 °C did not present an evident yield point, and the microstructure evolution mechanism was related with DGG. The grain size enlarged slightly with increasing strain, and thus the strain hardening behavior was observed in the whole process of hot compression.

(2) At 460 °C, the softening initiated by grain refinement and the hardening by grain growth reached a dynamic equilibrium. As a consequence, the stress-strain curve exhibits a plateau as the strain increases. Moreover, since the strength increased with decreasing temperature and the curve of 425 °C turns upwards, at stain of 0.4 an intersection appears between the curves of 425 °C and 460 °C.
(3) At the high temperature of 495 °C, the grains grew substantially at the initial stage of plastic deformation. In the subsequent deformation process, the grown grains were refined due to DRX at the central region and shear deformation region of the specimen. In this case, the corresponding curve exhibits a work softening behavior.

3.2.4. Grain growth mechanism

During hot deformation, the grain growth occurred readily in the extruded fine-grained Al or Mg matrix composites reinforced with ceramic particles [13,33,34]. However, the reason for grain growth was not discussed in the previous studies. It is well known that the driving force for grain growth is generally provided by the energy stored in grains and subgrain boundaries. Before hot compression, high energy was stored in the matrix by a large number of grain boundaries which derived from primary recrystallization during hot extrusion. The fine grains in this structure are highly susceptible to growth at elevated temperature. During static annealing the main factors affecting the grain growth usually include temperature, solutes and precipitated phase or reinforcements.

Generally, grains grow through movements of HAGBs. In this case, atom transfer at the boundaries between adjacent grains is controlled by thermal activation which depends on temperature significantly. Mobility of the boundaries increases with rising temperature, which obeys the Arrhenius equation [35].

$$M = M_0 \exp\left(-Q_b/RT\right) \tag{1}$$

where M is the mobility, M_0 a constant ($m^4/K\cdot mol$), and Q_b apparent activation energy for boundary migration (J/mol).

The dispersed particles commonly exert a retarding pressure on the LAGBs or HAGBs. Therefore, the particles have a pronounced effect on the processes of recovery, recrystallization, and grain growth. This effect is known as Zener drag [36]. In this work, the main second-phases in the matrix are $CuAl_2$ and α-Al(Fe, Mn)Si. The size and volume fraction of SiC reinforcement and second-phase particles are listed in Table 1. These statistical results were obtained by the graphic software on the micrographs. Due to the lower content of the second-phases, their inhibition of grain boundary migration is limited compared to SiC particles.

Fig. 4 shows that the grain size is associated with particle distribution due to pinning effect; however, it is difficult to give an accurate assessment for this. In a simplified model, the cubic particles are assumed to locate in a square lattice, and then the surface distance of the nearest neighbor particles λ can be evaluated by

$$\lambda = \frac{\left(1 - F_V^{1/3}\right)}{F_V^{1/3}} d \tag{2}$$

where F_v is the volume fraction of particles and d the diameter of particles. Substituting the average size of all particles (including SiC and second-phase) into Eq. (2) gives an average surface distance of ~13.3 μm, which is about 5.3 times of the initial grain size (~2.5 μm). Additionally, the distribution of particles in the composite was not completely uniform. As shown in Fig. 4c and e, in some regions the particle spacing exceeded ~50 μm. Thus, SiC particles could not pin grain boundaries in the whole region, and the grains in the regions with lower particle content grew rapidly as temperature exceeded the transition point of AGG.

Zener [36] suggested that the driving force of grain growth due to boundary curvature was counteracted by a pinning (drag) pressure from the particles on the boundary. The grain growth is inhibited completely when the grain size reaches a critical maximum diameter, i.e. Zener limit size D_c, which can be given by

$$D_C = \frac{4d}{3F_V} \tag{3}$$

where d is the diameter of the pinning particles and F_v the volume fraction of particles. Eq. (3) is known as the Zener equation, and its general form can be expressed as [37].

$$D_C = \frac{Kd}{F_V^m} \tag{4}$$

where K is a dimensionless constant unrelated to particle shape and m the exponent of F_v. Hillert [38] discussed the theoretical models and concluded that for the large volume fraction ($F_v > 0.1$), Eq. (4) was more appropriate when $K = 1.8$ and $m = 0.33$ were applied.

For the present 14 vol% SiCp/2014Al composite, the main pinning particles are SiC reinforcing particles, $CuAl_2$ precipitates, and α-Al(Fe,Mn)Si dispersoids. Using the total volume fraction and the weighted average diameters of particles in Table 1, the critical maximum diameter could be determined as $D_c = 52.9$ μm from Eq. (4) ($K = 1.8$, $m = 0.33$).

In general, the Zener limit refers to an equilibrium grain size after high temperature annealing. Rofman et al. [39] found that for the Al-4wt % Cu alloy in temperature range of 450–465 °C, the grain sizes in the specimens deformed at low strain rates (10^{-3}, 10^{-4} s^{-1}) were larger than that annealed with the same time. This implies that the strain-induced grain boundary mobility promotes the grain growth substantially. The equilibrium state grain size after static annealing should be a lower limit at high temperature. Therefore, using the D_c in Eq. (4) we can qualitatively evaluate whether the grain size is stable during hot deformation.

In this work, the initial grain size of 2.5 μm is far less than the critical maximum dimension of 52.9 μm. Thus, it is reasonable that the microstructure of the matrix was unstable and AGG occurred at high temperature (~T_{agg}).

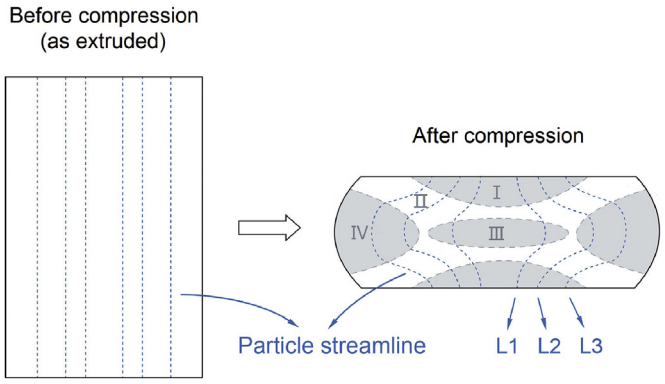

Fig. 6. Schematic diagram of the deformation region partition and streamline distribution in the compressed specimen (I Hard-to-deform region; II Shear deformation region; III Compressive deformation region; IV Lateral region).

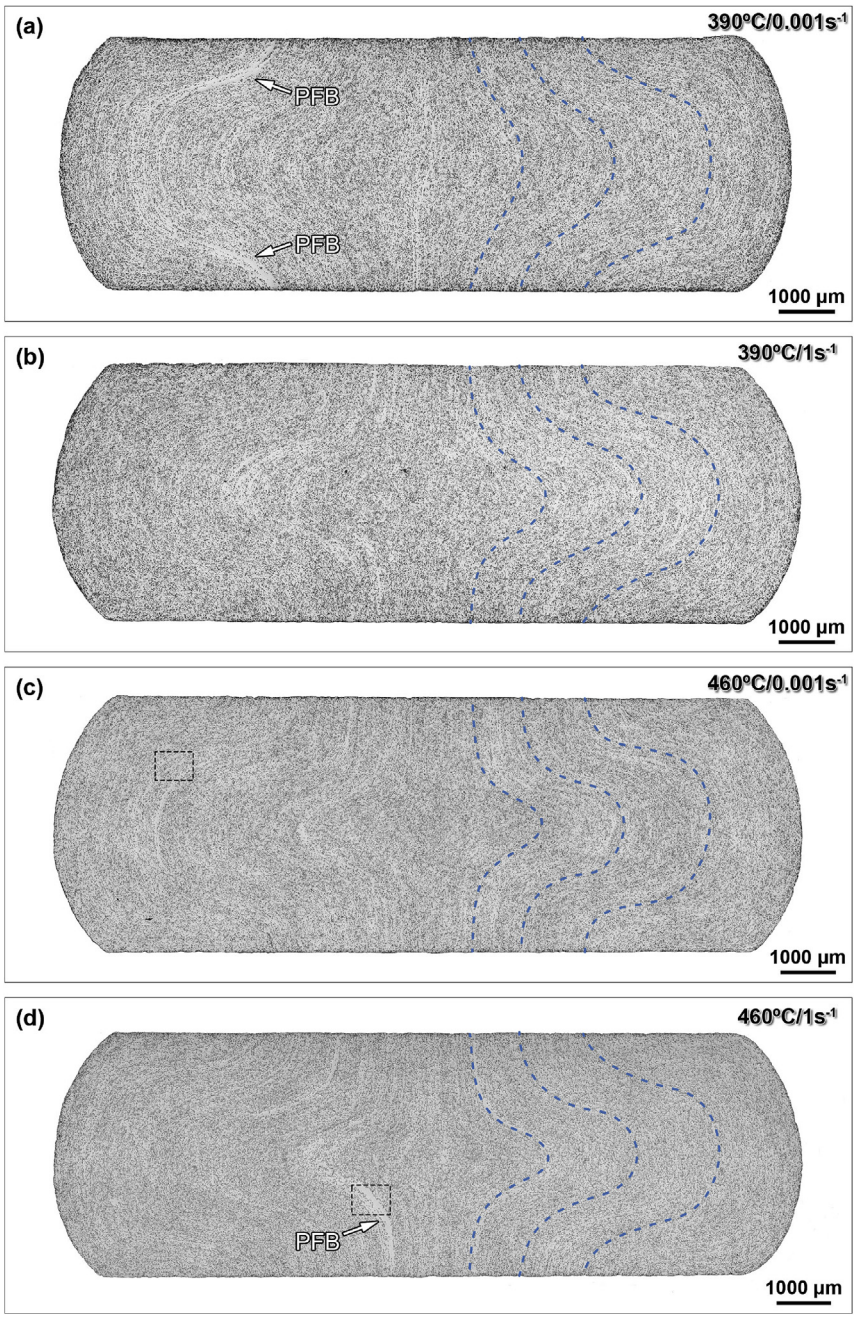

Fig. 7. Overall distribution of SiCp in longitudinal cross-section of the specimens compressed with true strain 0.9: (a) at 390 °C/0.001 s^{-1}, (b) at 390 °C/1 s^{-1} (c) at 460 °C/0.001 s^{-1}, (d) at 460 °C/1 s^{-1} (particle streamline denoted by the dash line).

3.3. Evolution of SiC particle distribution during hot working

During hot working, SiC particles moved with the flow of matrix so as to accommodate plastic deformation of adjacent matrix by changing orientation rather than interface sliding. High strain gives rise to a significant rearrangement of particles. For the PRAMCs fabricated by casting method, the aluminum matrix tends to presents a certain texture along the stirring axis [40] and the grain size of the matrix is relatively large. Moreover, the reinforcing particles were distributed not only on the grain boundaries but also within the grain interiors [41]. After hot extrusion the PRAMCs fabricated by casting method tended to form a relatively regular distribution of reinforcing particles [42] compared with the composite fabricated by powder metallurgy technique [43]. This string-like structure or particle streamlines (shown in Fig. 1a) can be weakened or broadened under specific hot working conditions.

3.3.1. Distribution of SiC particle streamline related to temperatures and strain rates

3.3.1.1. Pattern of SiC particle streamlines. Fig. 6 shows a schematic diagram of deformation regions and particle streamline distribution in the compressed specimen. The longitudinal section of the specimen can be partitioned into four regions (Regions I, II, III, IV) according to the differences in stress states and accumulated strain during hot deformation. Furthermore, on the sections of specimens before and after compression particle streamlines were marked by trace lines of L1, L2 and L3 to indicate the flow regimes of particles at various locations.

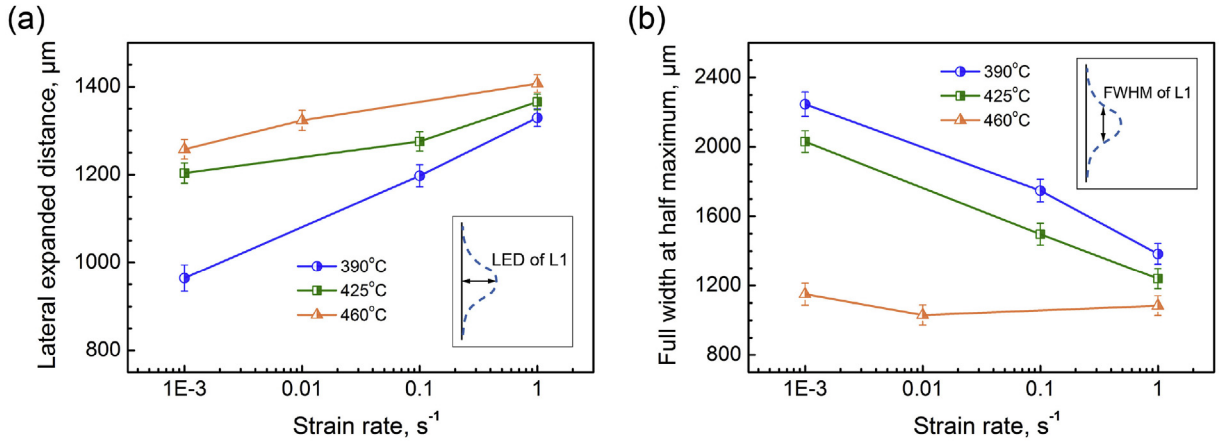

Fig. 8. Size variation of trace line 'L1' with temperatures and strain rates under true strain 0.9: (a) lateral expanded distance (LED), (b) full width at half maximum (FWHM).

Fig. 7 shows the distribution of SiC particle streamlines at some typical compression parameters. The streamlines were quite different with the variant compression parameters, as denoted by the trace lines. Near the center region the bulging of streamline L1 tended to concentrate in the middle with temperature increase, which is related to a strain concentration in the compressive deformation region (Region III in Fig. 6). Note that L2 and L3 which were across Regions I, II and IV also presented similar situations. Furthermore, comparing the overall distribution of SiC particles under various parameters in Fig. 7, it can be seen that the uniformity of SiC particles was associated with strain. In Region III with large plastic strain, the particle streamlines essentially vanished at all hot deformation parameters.

In order to investigate the effect of processing parameters on deformation uniformity, the lateral expanded distance (LED) and the full width at half maximum (FWHM) of trace line L1 were measured for analysis, as shown in Fig. 8. It is clear that at 390 °C the LED increased and the FWHM decreased with rising strain rate, and the size variation of the trace line was larger than those at higher temperatures. This indicates that at the lower temperature of 390 °C, the higher strain rate caused the compressive deformation to concentrate in the middle of specimens, while the lower strain rate was helpful to improve deformation uniformity. At 460 °C, the LED presented a larger magnitude while the FWHM

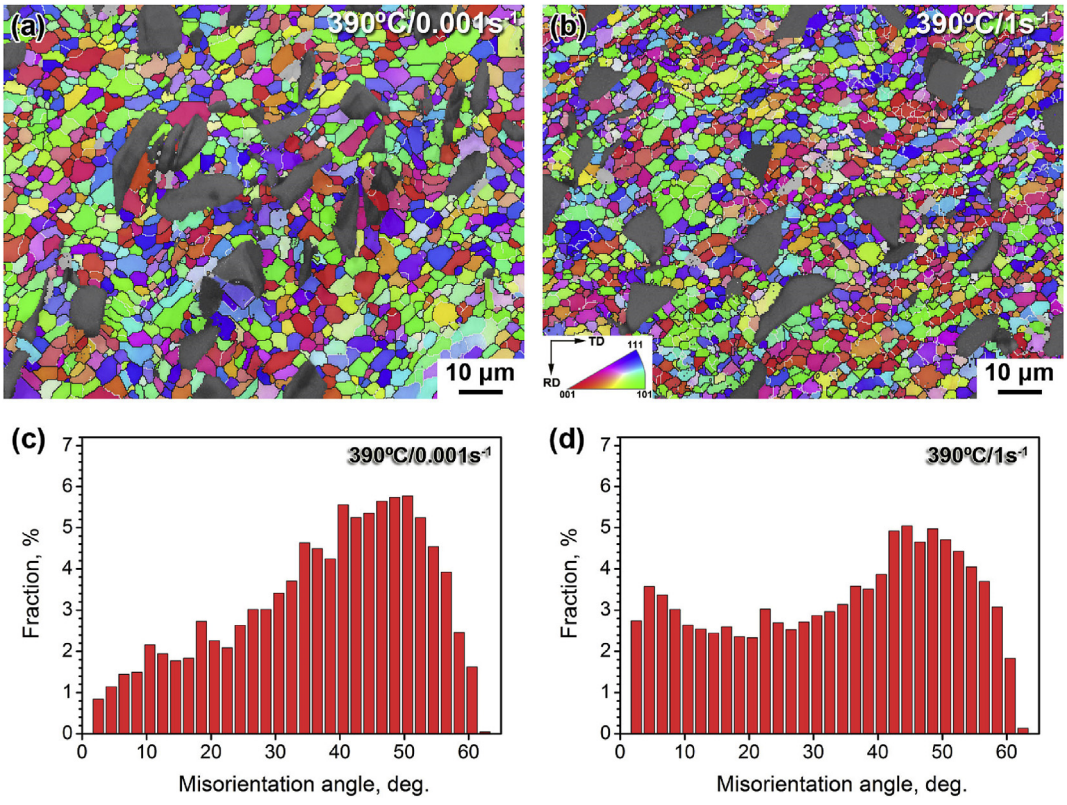

Fig. 9. EBSD results of shear deformation region with true strain 0.9: grain micrographs (IPF color + grain boundary) at (a) 390 °C/0.001 s^{-1}, (b) 390 °C/1 s^{-1}; distribution of misorientation angles at (c) 390 °C/0.001 s^{-1}, (d) 390 °C/1 s^{-1}. (For interpretation of the references to color in this figure legend, the reader is referred to the Web version of this article.)

became smaller, and also the fluctuations of LED and FWHM were quite small with changing strain rates. These imply that even at lower strain rate, the higher temperature still tended to induce a strain concentration in the center region.

3.3.1.2. The relevant matrix structure under specific conditions. In general, at the lower deformation temperatures (<400 °C), the grain boundaries are hardly shown distinctly by metallography method due to existence of SiC particles. By contrast, the EBSD

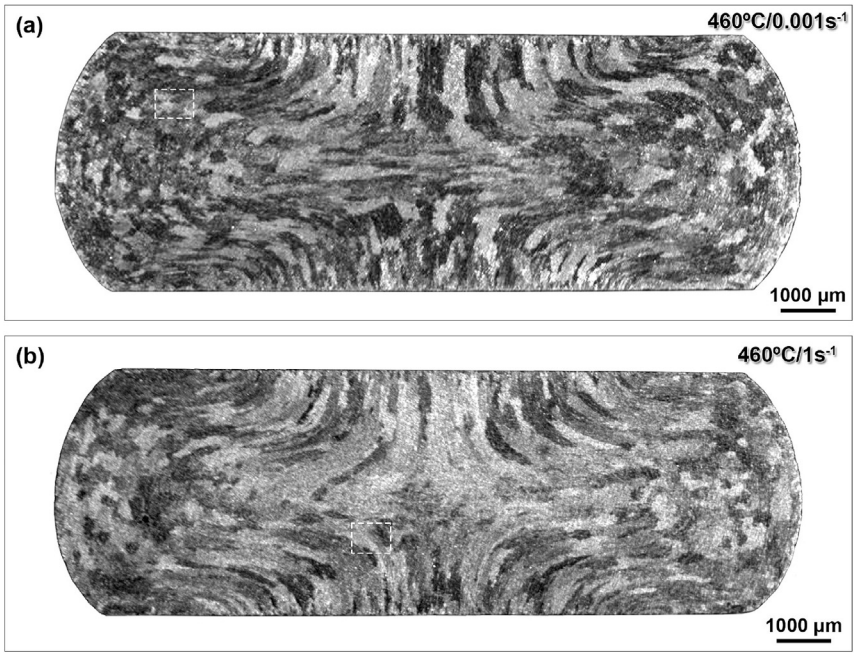

Fig. 10. Grain structure in longitudinal cross-section of the specimens compressed with true strain 0.9: (a) at 460 °C/0.001 s^{-1}, (b) at 460 °C/1 s^{-1}.

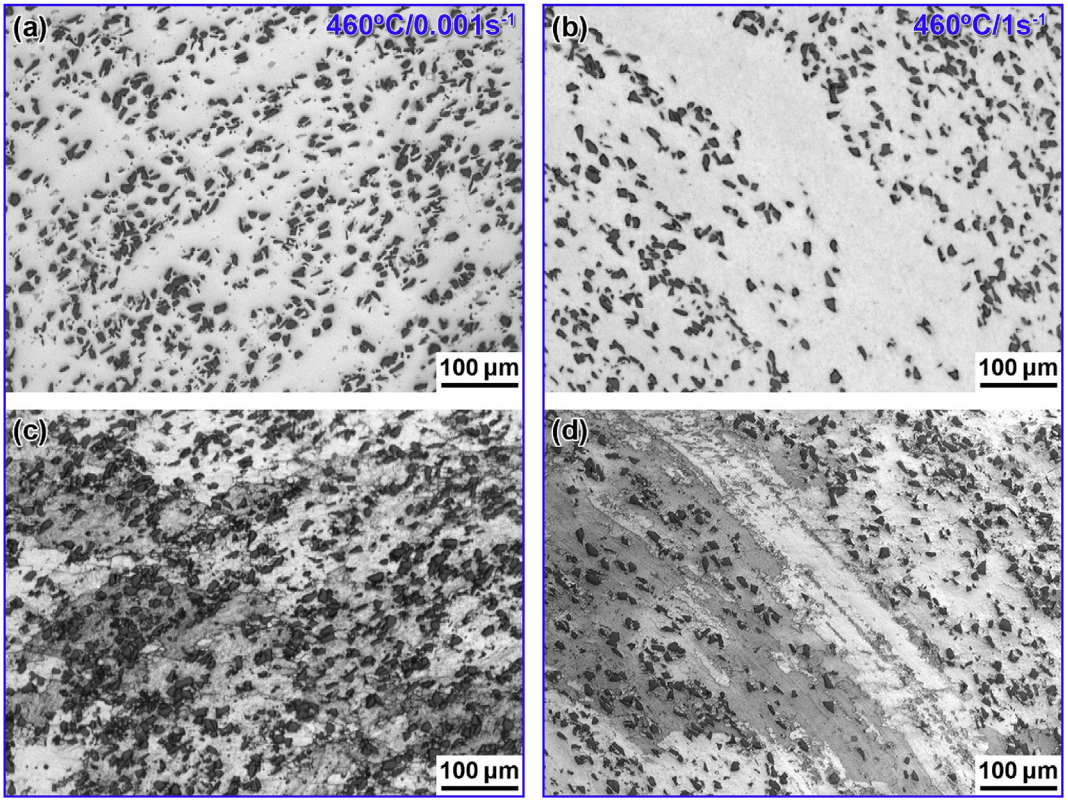

Fig. 11. Morphologies of PFBs in longitudinal cross-section of specimens compressed with true strain 0.9: (a) at 460 °C/0.001 s^{-1} (local region in the dotted box of Fig. 7(c)), (b) at 460 °C/1 s^{-1} (local region in the dotted box of Fig. 7(d)), (c) etched metallograph corresponding to (a), (d) etched metallograph corresponding to (b).

maps of Fig. 9a and b shows the clear grain structures in the shear deformation region at 390 °C. Due to the sufficient restoration time, LAGBs at 390 °C and 0.001 s^{-1} were less than that at 390 °C and 1 s^{-1}, as shown in Fig. 9c and d. The grain sizes under these two parameters were 3.0 and 2.7 μm respectively, which did not change obviously compared to the initial grain size of as-received composite (~2.5 μm). Therefore, DRV was the dominant deformation mechanism at 390 °C. DRV produces elongated grain instead of refined and equiaxed grains [44]. The as-received composite has fine grain which is close to the lower limit of subgrain size [22]. In this situation, dislocations were inclined to move toward the grain boundaries.

Fig. 10a and b shows coarsened grain structures after AGG at the higher temperature of 460 °C. It was noted that the morphology of the coarsened grains had a good agreement with the distribution of SiC particle streamlines in Fig. 7c and d. The mechanism of AGG is a strain induced grain boundary migration. During hot deformation, SiC particles moved with the plastic flow of the matrix, while the SiC particle band had a hindering effect on the migration of grain boundaries simultaneously. In the transverse direction of streamlines, the pinning pressure of particle band on the grain boundaries was stronger and therefore the grain boundaries migrated more readily along the streamlines. As a result, the grains and SiC particle streamline exhibited the identical distribution pattern.

3.3.2. *Structural characteristics of streamline and particle free band*

During hot compression, at some regions the streamlines formed by extrusion broadened and developed into particle free bands (PFBs). The local morphologies of streamlines and PFBs are shown in Fig. 11, which corresponds to the dotted box region in Fig. 7c and d. In Fig. 11a, the width of streamlines was about 50 μm which is close to the maximum spacing of particles in the as-received composite. In Fig. 11b, the broad PFBs reached up to about 150 μm which can actually be identified by the macroscopic observation. In the streamlines and PFBs the long axis of SiC particles was approximately parallel to the flow direction.

Figs. 11c and d shows the grain structures around streamlines and PFBs (the same regions in Fig. 11a and b). In the region of the streamlines (Fig. 11c), after grain growth the alignment of the grain boundaries was not completely consistent with the streamlines. However, in the region of the PFBs (Fig. 11d), the grain size was very large and the grain boundaries were aligned approximately parallel to the PFBs. The pinning effect of particles on the grain boundaries did not exist in the PFB interior. In this case, the grains grew significantly and the grain boundaries readily migrated along the direction parallel to the PFBs.

3.3.3. *Evolution of particle streamlines under different strain states*

Fig. 12 shows the schematic diagram of particle streamlines under different deformation states. In the hard-to-deform region (Region I in Fig. 6), the particle orientation generally does not change under small compressive strain. Thus, the lateral spacing of adjacent particles increases and the longitudinal spacing of particles narrows simultaneously. In this case, the distance of initial

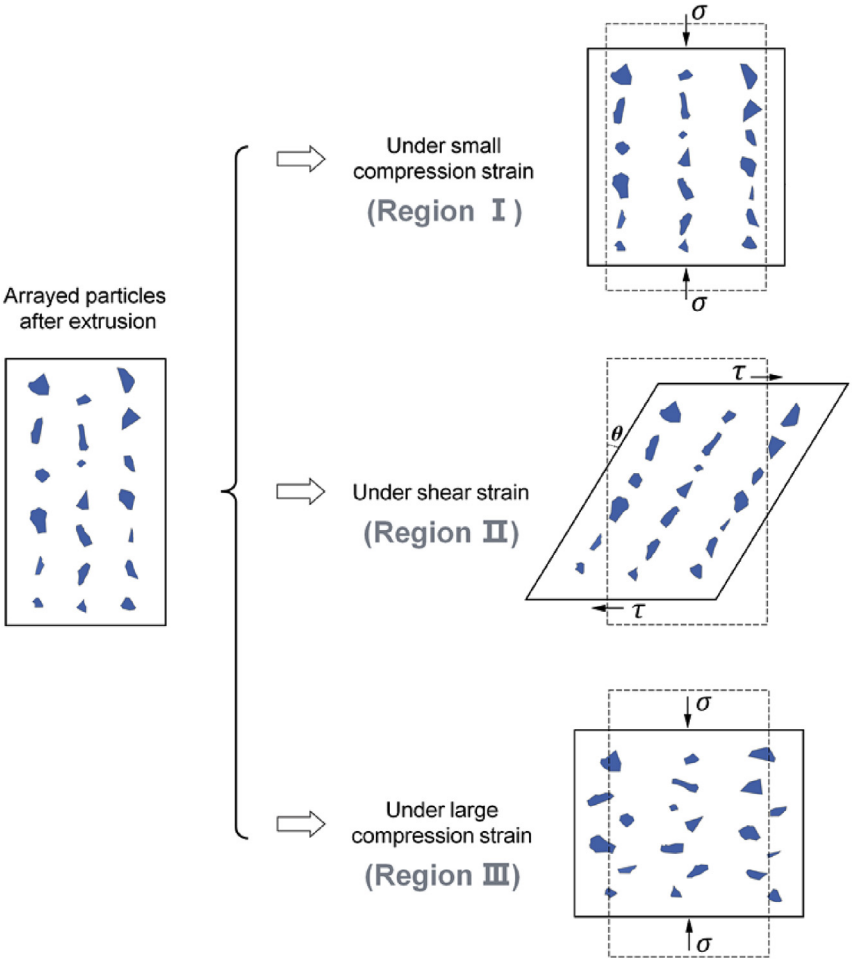

Fig. 12. Schematic diagram of the evolution of particle streamline under different deformation states.

particle streamlines would broaden and be likely to develop into the PFBs.

In the shear deformation region (Region II in Fig. 6), the compressive strain is also rather limited, which provides a potential condition for PFB forming. In this region the particles rotate with the flow of the matrix, and keep parallel to the shear direction. As shown in Fig. 12, the tilt angle θ is directly proportional to the magnitude of shear strain.

In the compressive deformation region (Region III in Fig. 6), under large compressive strain the particles will be further close to each other in the longitudinal direction. Ashby suggested that the geometrically-necessary dislocations would generate in alloys to accommodate the gradients of plastic deformation between the particles and matrix [45]. During the hot working of the composites, the hard particles constrained the deformation of adjacent matrix, and then a stagnant layer formed around the particles. When the distance reaches the thickness of stagnant layer, the particles will maintain the compatible deformation in a manner of rotation. More importantly, in this center region which is subjected to the squeezing from up and down sides, the lateral flow of the matrix will lead to a transverse arrangement of the particles. Consequently, the wide particle streamlines and PFBs would be broken up in the compressive deformation region.

3.3.4. *Influence of deformation parameters on PFBs*

In Fig. 7a and d, it can be found that the PFBs were all located in the hard-to-deform region and shear deformation region (as denoted by the arrows). At 390 °C/0.001s^{-1} (Fig. 7a), two wide PFBs were symmetrically situated near the upper and lower end surfaces where strain was small. Considering the symmetric distribution, it can be speculated that these two PFBs formed in the extruding and incipient compressing processes might be a continuous strip across the specimen section. However, because of the relatively large compressive strain at the lateral region (Region IV in Fig. 6), this continuous PFBs were locally eliminated.

As shown in Fig. 7d, there was a wide PFB situated near the center of the hard-to-deform region (Region I in Fig. 6). In view of the conclusion in section 3.3.1.1 the condition of 460 °C/1s^{-1} is a deformation parameter which can improve the uniformity of SiC particle distribution, but the PFBs cannot be eliminated in the hard-to-deform region and shear deformation region. This indicates that the elimination of PFBs mainly depends on the enhancement of strain rather than the temperature and strain rate.

4. Conclusions

Based on the hot compression test of 14 vol% SiCp/2014Al composite, the anomalous behavior of stress-strain curves and the distribution of reinforcing particles during hot deformation were investigated. The main conclusions are as follows:

(1) For the fine-grained 14 vol% SiCp/2014Al composites, the yield strength at 460 °C and 495 °C was higher than that at 425 °C under the low strain rate of 0.001 s^{-1}. This anomalous behavior is caused by the multiple impediments to GBS and intragranular slip by AGG and intragranular SiC particles respectively.

(2) The Zener drag effect of reinforcing particles on the grain boundaries was quite limited for the fine-grained composite. Because the strain induced grain boundary migration promotes the grain growth, the Zener limit dimension can be used to qualitatively evaluate the potential of AGG during hot working.

(3) The increase in temperature and strain rate tended to result in the strain concentration (or localization). During AGG, the grain boundaries migrated more readily along the particle streamlines which is of the lower resistance.

(4) The particle streamlines could weaken or develop into the particle free bands under specific hot deformation conditions. The particle free bands generally were situated at the hard-to-deform region and shear deformation region which were subjected the monotonous and small plastic stain.

Acknowledgements

The authors gratefully acknowledge the support of National Key R & D Program of China (No. 2017YFB0703104). The authors also thank Prof. Q. B. Ouyang from Shanghai Jiao Tong University for providing the samples of 14 vol% SiCp/2014Al composites.

References

[1] R.J. Arsenault, R.M. Fisher, Microstructure of fiber and particulate SiC in 6061 Al composites, Scripta Met. 17 (1983) 67–71.
[2] J.C. Shao, B.L. Xiao, Q.Z. Wang, Z.Y. Ma, Y. Liu, K. Yang, Constitutive flow behavior and hot workability of powder metallurgy processed 20 vol.%SiCp/2024Al composite, Mater. Sci. Eng. A 527 (2010) 7865–7872.
[3] Z.W. Wang, M. Song, C. Sun, Y.H. He, Effects of particle size and distribution on the mechanical properties of SiC reinforced Al–Cu alloy composites, Mater. Sci. Eng. A 528 (2011) 1131–1137.
[4] A.J. Knowles, X. Jiang, M. Galano, F. Audebert, Microstructure and mechanical properties of 6061 Al alloy based composites with SiC nanoparticles, J. Alloys Compd. 615 (2014) S401–S405.
[5] C. Xue, J.K. Yu, Enhanced thermal transfer and bending strength of SiC/Al composite with controlled interfacial reaction, Mater. Des. 53 (2014) 74–78.
[6] J.A. Liu, Q.X. Qu, Y. Liu, R.G. Li, B. Liu, Compressive properties of Al-Si-SiC composite foams at elevated temperatures, J. Alloys Compd. 676 (2016) 239–244.
[7] A. Evans, C. San Marchi, A. Mortensen, Metal Matrix Composites in Industry: an Introduction and a Survey, Kluwer Academic Publishers, Boston, 2003.
[8] M. Furukawa, Y. Miura, M. Nemoto, The effect of temperature on the yield stress of Al-Li alloy, Trans. Jpn. Inst. Met. 26 (1985) 414–422.
[9] M. Furukawa, Y. Miura, M. Nemoto, Temperature and strain rate dependences of yield stress of an Al-Li-Cu-Mg-Zr alloy, Trans. Jpn. Inst. Met. 28 (1987) 655–665.
[10] Y. Miura, K. Yusu, M. Furukawa, M. Nemoto, Temperature dependence of yield strength of Al-Li single crystals, J. Phys. Colloq. 48 (1987) 549–555.
[11] D.P. Pope, S.S. Ezz, Mechanical properties of Ni3Al and nickel-base alloys with high volume fraction of γ', Int. Met. Rev. 29 (1984) 136–167.
[12] H. Yang, Z.H. Li, M.S. Huang, Modeling of abnormal mechanical properties of nickel-based single crystal superalloy by three-dimensional discrete dislocation dynamics, Modell. Simul. Mater. Sci. Eng. 22 (2014), 085009.
[13] S.Y. Wang, Q. Tang, D.J. Li, J.X. Zou, X.Q. Zeng, Q.B. Ouyang, W.J. Ding, The hot workability of SiCp/2024 Al composite by stir casting, Mater. Manuf. Processes 30 (2015) 624–630.
[14] J. Lewandowski, C. Liu, W. Hunt, Effects of matrix microstructure and particle distribution on fracture of an aluminum metal matrix composite, Mater. Sci. Eng. A 107 (1989) 241–255.
[15] P.A. Karnezis, G. Durrant, B. Cantor, Characterization of reinforcement distribution in cast Al-Alloy/SiCp composites, Mater. Charact. 40 (1998) 97–109.
[16] J. Boselli, P.J. Gregson, I. Sinclair, Quantification of particle distribution effects on fatigue in an Al–SiCp composite, Mater. Sci. Eng. A 379 (2004) 72–82.
[17] D. Zhang, K. Sugio, K. Sakai, H. Fukushima, O. Yanagisawa, Effect of spatial distribution of SiC particles on the tensile deformation behavior of Al-10 vol% SiC composites, Mater. Trans. 48 (2007) 171–177.
[18] J.C. Healy, C.J. Beevers, A study of fatigue crack growth in a particulate-reinforced Al-Si alloy at 23 and 220 °C, Mater. Sci. Eng. A 142 (1991) 183–192.
[19] S. Kumai, J.E. King, J.F. Knott, Fatigue crack growth behaviour in molten-metal processed SiC particle-reinforced aluminium alloys, Fatig. Fract. Eng. Mater. Struct. 15 (1992) 1–11.
[20] T. Feng, X.Z. Chen, L.H. Wu, S.N. Lou, Diffusion welding of SiCp/2014Al composites using Ni as interlayer, J. Univ. Sci. Technol. Beijing 13 (2006) 267–271.
[21] Y.S. Su, Q.B. Ouyang, W.L. Zhang, Z.Q. Li, Q. Guo, G.L. Fan, D. Zhang, Composite structure modeling and mechanical behavior of particle reinforced metal matrix composites, Mater. Sci. Eng. A 597 (2014) 359–369.
[22] A. Gholinia, F. Humphreys, P. Prangnell, Production of ultra-fine grain microstructures in Al-Mg alloys by conventional rolling, Acta Mater. 50 (2002) 4461–4476.
[23] G. Davignon, B. Verlinden, L. Delaey, A. Serneels, An isothermal section at 550 °C in the Al-Rich corner of the Al-Fe-Mn-Si system, Metall. Mater. Trans. A 27 (1996) 3357–3361.
[24] K.-T. Park, F.A. Mohamed, Creep strengthening in a discontinuous SiC-Al composite, Metall. Mater. Trans. A 26 (1995) 3119–3129.
[25] Z.G. Lin, F.A. Mohamed, Creep and microstructure in powder metallurgy 15 vol.% SiCp-2009 Al composite, J. Mater. Sci. 47 (2012) 2975–2984.

[26] Z.Y. Huang, X.X. Zhang, B.L. Xiao, Z.Y. Ma, Hot deformation mechanisms and microstructure evolution of SiCp/2014Al composite, J. Alloys Compd. 722 (2017) 145–157.
[27] W.J. Li, B. Cai, Y.C. Wang, Z.X. Liu, S. Yang, Creep of Al–0.2Sc–0.04Zr alloys after different cold-rolling and ageing combinations, Mater. Sci. Eng. A 615 (2014) 148–152.
[28] R.S. Kottada, A.H. Chokshi, Grain boundary sliding during diffusion and dislocation creep in a Mg-0.7 Pct Al alloy, Metall. Mater. Trans. A 38 (2007) 1743–1749.
[29] F. Mokdad, D.L. Chen, Z.Y. Liu, D.R. Ni, B.L. Xiao, Z.Y. Ma, Hot deformation and activation energy of a CNT-reinforced aluminum matrix nanocomposite, Mater. Sci. Eng. A 695 (2017) 322–331.
[30] F. Mokdad, D.L. Chen, Z.Y. Liu, D.R. Ni, B.L. Xiao, Z.Y. Ma, Three-dimensional processing maps and microstructural evolution of a CNT-reinforced Al-Cu-Mg nanocomposite, Mater. Sci. Eng. A 702 (2017) 425–437.
[31] M.L. Olguín-González, D. Hernández-Silva, M.A. García-Bernal, V.M. Sauce-Rangel, Hot deformation behavior of hot-rolled AZ31 and AZ61 magnesium alloys, Mater. Sci. Eng. A 597 (2014) 82–88.
[32] H. Somekawa, T. Tanaka, H. Sasaki, K. Kita, A. Inoue, K. Higashi, Diffusion bonding in ultra fine-grained Al–Fe alloy indicating high-strain-rate superplasticity, Acta Mater. 52 (2004) 1051–1059.
[33] T. Zhong, K.P. Rao, Y.V.R.K. Prasad, F. Zhao, M. Gupta, Hot deformation mechanisms, microstructure and texture evolution in extruded AZ31–nano-alumina composite, Mater. Sci. Eng. A 589 (2014) 41–49.
[34] K.K. Deng, J.C. Li, F.J. Xu, K.B. Nie, W. Liang, Hot deformation behavior and processing maps of fine-grained SiCp/AZ91 composite, Mater. Des. 67 (2015) 72–81.
[35] Y. Huang, F.J. Humphreys, Measurements of grain boundary mobility during recrystallization of a single-phase aluminium alloy, Acta Mater. 47 (1999) 2259–2268.
[36] C.S. Smith, Grains, phases, and interphases: an interpretation of microstructure, Trans. Metall. Soc. AIME 175 (1948) 15–51.
[37] P.A. Manohar, M. Ferry, T. Chandra, Five decades of the Zener equation, ISIJ Int. 38 (1998) 913–924.
[38] M. Hillert, Inhibition of grain growth by second-phase particles, Acta Metall. 36 (1988) 3177–3181.
[39] O. Rofman, P. Bate, I. Brough, F. Humphreys, Study of dynamic grain growth by electron microscopy and EBSD, J. Microsc. 233 (2009) 432–441.
[40] J. Sheng, L.D. Wang, Y. Zhao, S.C. Xu, X.L. Liu, W.D. Fei, Effect of solution treatment on the texture and tensile properties of Mg2B2O5W/2024Al composite, J. Alloys Compd. 701 (2017) 716–721.
[41] L. Ceschini, G. Minak, A. Morri, Forging of the AA2618/20 vol.% Al2O3p composite: effects on microstructure and tensile properties, Compos. Sci. Technol. 69 (2009) 1783–1789.
[42] B. Dutta, I. Samajdar, M.K. Surappa, Particle redistribution and matrix microstructure evolution during hot extrusion of cast SiCp reinforced aluminium alloy matrix composites, Mater. Sci. Technol. 14 (1998) 36–46.
[43] Z.Y. Liu, Q.Z. Wang, B.L. Xiao, Z.Y. Ma, Y. Liu, Experimental and modeling investigation on SiCp distribution in powder metallurgy processed SiCp/2024 Al composites, Mater. Sci. Eng. A 527 (2010) 5582–5591.
[44] F.J. Zhu, H.Y. Wu, S. Lee, M.C. Lin, D. Chen, Dynamic behavior of a 6069 Al alloy under hot compression, Mater. Sci. Eng. A 640 (2015) 385–393.
[45] M.F. Ashby, The deformation of plastically non-homogeneous materials, Philos. Mag. 21 (1970) 399–424.